

## Supporting Information

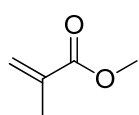
### **Metallo-Folded Single-Chain Nanoparticles with Catalytic Selectivity**

*Ana Sanchez-Sanchez, Arantxa Arbe, Juan Colmenero and José A.  
Pomposo\**

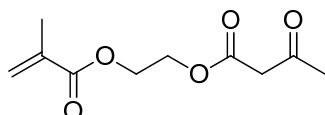
*\*E-mail: [josetxo.pomposo@ehu.es](mailto:josetxo.pomposo@ehu.es)*

## 1. Materials and Methods

Methyl methacrylate (**MMA**) (99%), (2-acetoacetoxy)ethyl methacrylate (**AEMA**) (95%), 2,2-azobis(2-methylpropionitrile) ( $\geq 98\%$ ), copper (II) acetate ( $\text{Cu}(\text{OAc})_2$ ) (98%), copper (II) chloride (**1**) (anhydrous, powder,  $\geq 99.995\%$  trace metals basis), copper(II) acetylacetonate ( $\geq 99.99\%$  trace metals basis), copper (I) bromide ( $\text{CuBr}$ ) (99.999% trace metal basis), propargyl acetate (**2a**) (98%), 1-octyn-3-ol (**3a**) (96%), propargyl benzoate (**4a**) (98%), propargyl acrylate (**7a**) (98%), propargyl 2-bromoisobutyrate (**8a**) ( $> 97\%$ ), phenyl propargyl ether (**9a**) ( $\geq 90\%$ ), 3-butynyl 2-bromoisobutyrate (**10a**) (97%, (GC)), ethyl acetate (anhydrous, 99.8 %), diethyl ether (ACS reagent, anhydrous,  $> 99.0\%$ ), chloroform ( $\geq 99\%$ ), deuterated *N,N*-dimethylformamide ( $\text{DMF-d}_7$ ) (99.5 atom % D), deuterated benzene (benzene- $\text{d}_6$ ) (99.5 atom % D), deuterated toluene (toluene- $\text{d}_8$ ) (99.6 atom % D) and deuterated chloroform ( $\text{CDCl}_3$ ) (99.96 atom % D, containing 0.03 % (v/v) tetramethylsilane, TMS) were purchased from Aldrich and used, unless specified, as received. 3-cyclohexyl-1-propyne (**5a**) (97%), propargyl propionate (**6a**) (98%) and benzyl azide (94%) were purchased from Alfa Aesar. 2-Cyanoprop-2-yl-dithiobenzoate (CPDB) ( $\geq 97\%$ ) was purchased from Strem Chemicals. Methanol ( $\text{MeOH}$ ) (synthesis grade) and tetrahydrofuran (THF) (HPLC grade) were purchased from Scharlab. Methyl-5-hexynoate (**11a**) (95%) was purchased from Acros Organics. MMA was purified by distillation before use. AEMA was purified by passing through basic alumina.



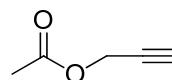
**MMA**



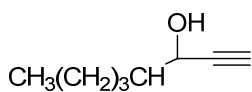
**AEMA**



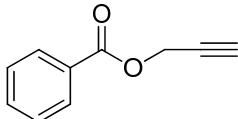
**1**



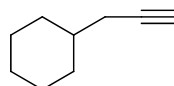
**2a**



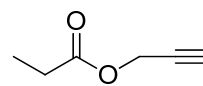
**3a**



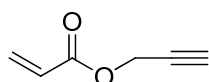
**4a**



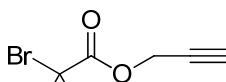
**5a**



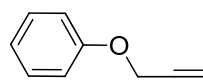
**6a**



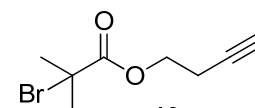
**7a**



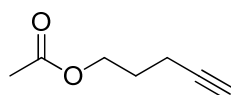
**8a**



**9a**

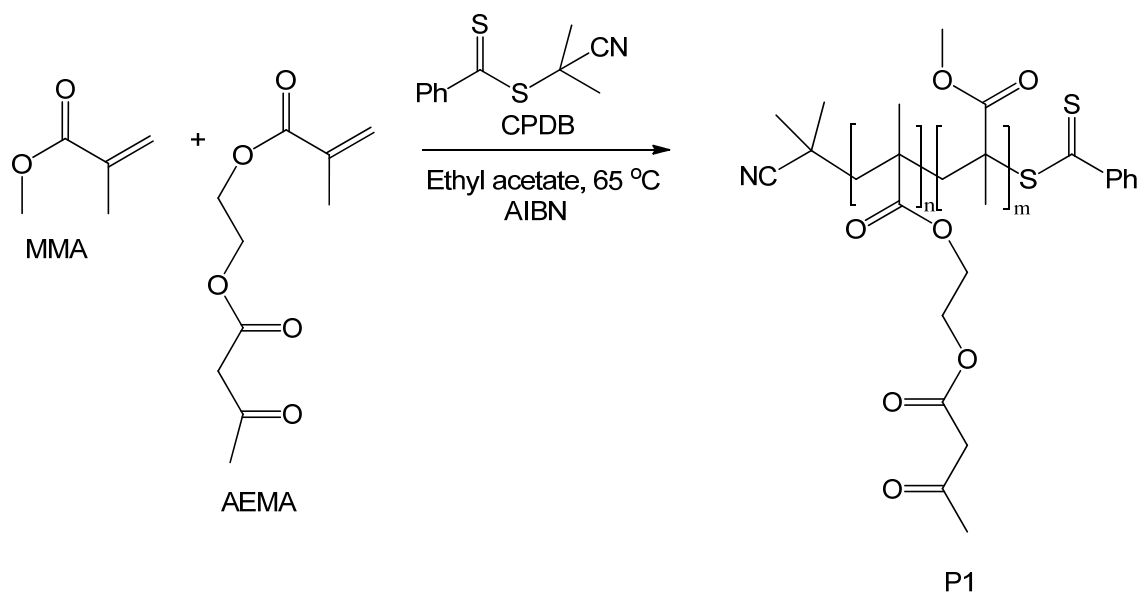


**10a**

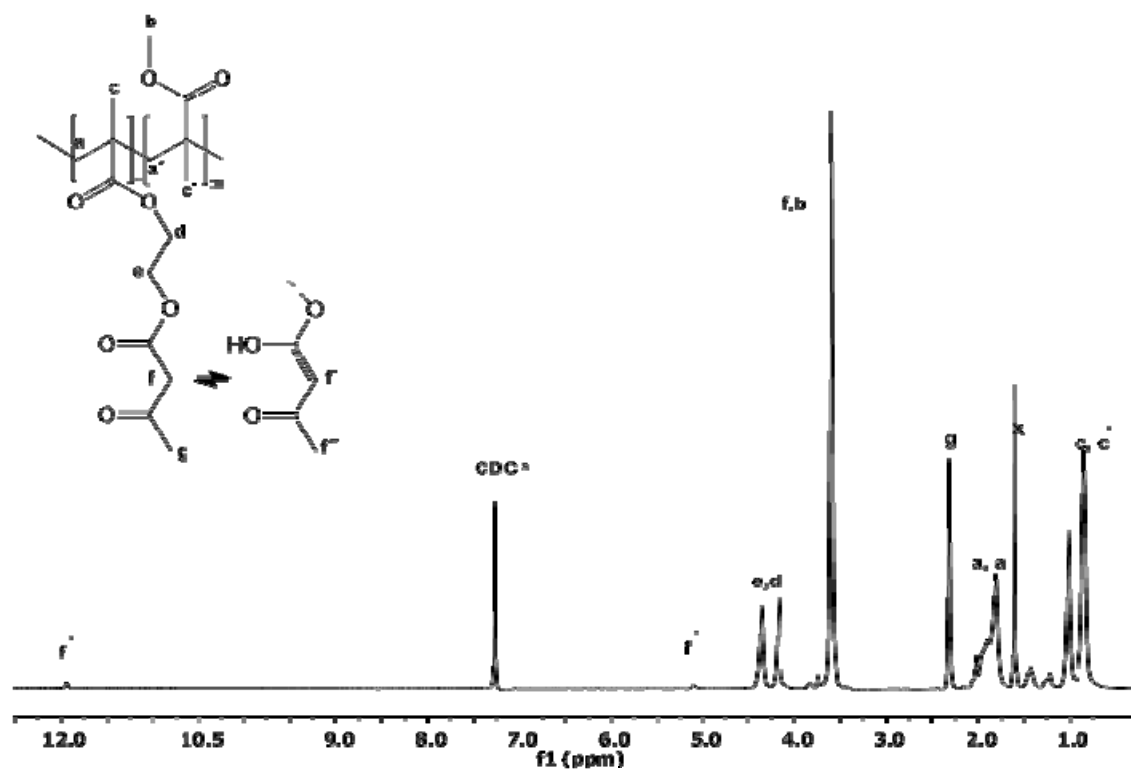


**11a**

**Synthesis of precursors:** In a typical procedure, MMA (1 ml, 9.4 mmol), AEMA (0.6 ml, 3.1 mmol), CPDB (0.8 mg,  $3 \times 10^{-2}$  mmol) and 2,2-azobis(2-methylpropionitrile) (1 mg,  $3 \times 10^{-2}$  mmol) were dissolved in ethyl acetate (3.2 ml). The reaction mixture was degassed by passing argon for 15 min. The copolymerization reaction was carried out at 65 °C for 18 h. The resulting nanoparticle precursor was isolated by precipitation in methanol and further drying (**P1**: Yield (%) = 72,  $M_w$  (SEC/MALLS,  $dn/dc = 0.083$ ) = 375 kDa,  $M_w/M_n = 1.4$ ,  $R_g = 26 \pm 1.4$  nm, composition ( $^1\text{H NMR}$ ) = 30 mol% AEMA).

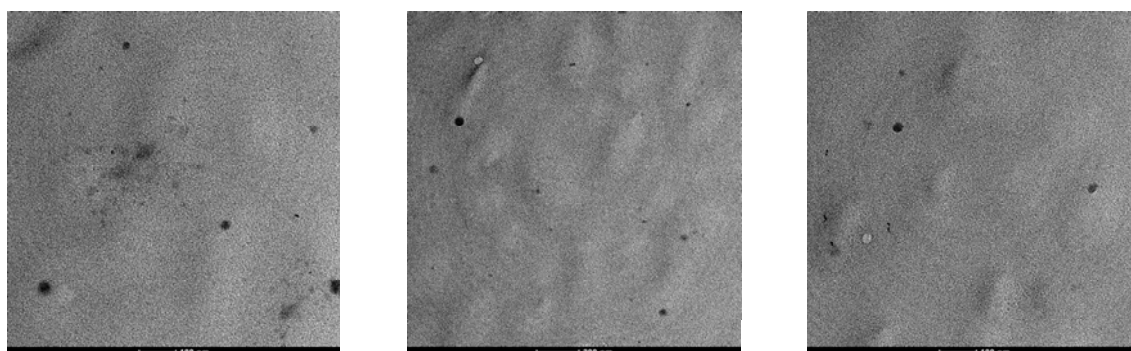
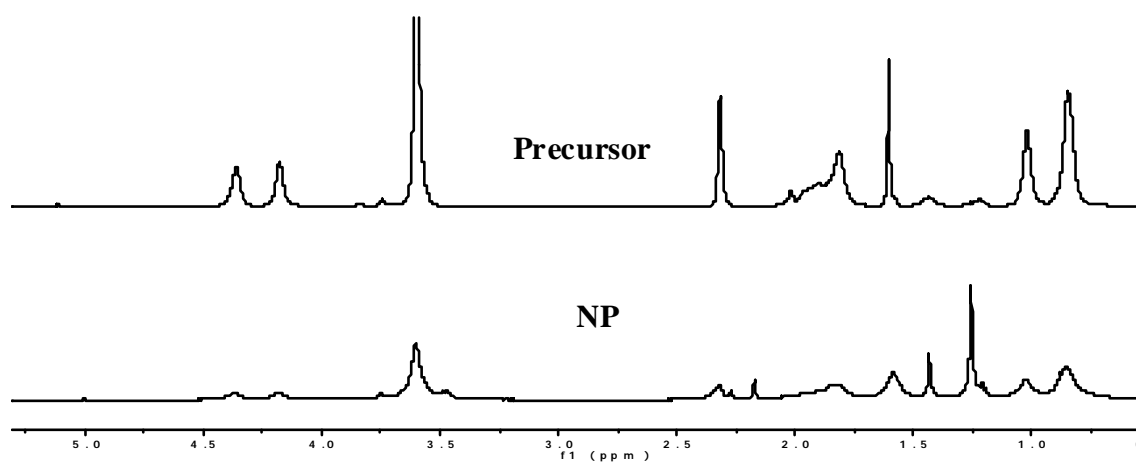


The <sup>1</sup>H NMR spectrum in CDCl<sub>3</sub> of precursor **P1** and the corresponding proton assignments is shown below:



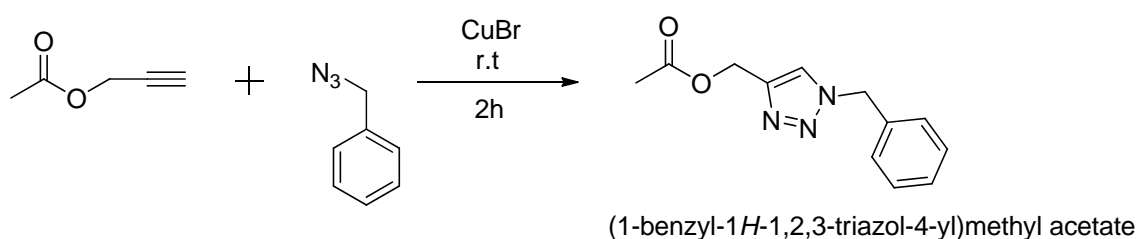
**Synthesis of metallo-folded nanoparticles:** In a typical reaction, the precursor (**P1**, 150 mg, 0.32 mmol) was dissolved in THF (150 ml) at room temperature. Then, a solution of  $\text{Cu}(\text{OAc})_2$  (15 mg, 0.08 mmol Cu) in THF was progressively added, and the mixture was maintained under stirring for 24 h. Finally, the metallo-folded SCNP **NP1** was isolated by precipitation in diethyl ether and further drying under dynamic vacuum. The progressive folding/collapse process was followed through simultaneous SEC/MALLS measurements. (**NP1**: Yield (%) = 71,  $M_w$  (SEC/ MALLS,  $dn/dc=0.083$ ) = 390 kDa,  $M_w/M_n = 1.3$ ,  $R_g = 15 \pm 1.1$  nm).

A comparison of the  $^1\text{H}$  NMR spectra in  $\text{CDCl}_3$  of **P1** and **NP1** and representative TEM images of **NP1** are shown below:

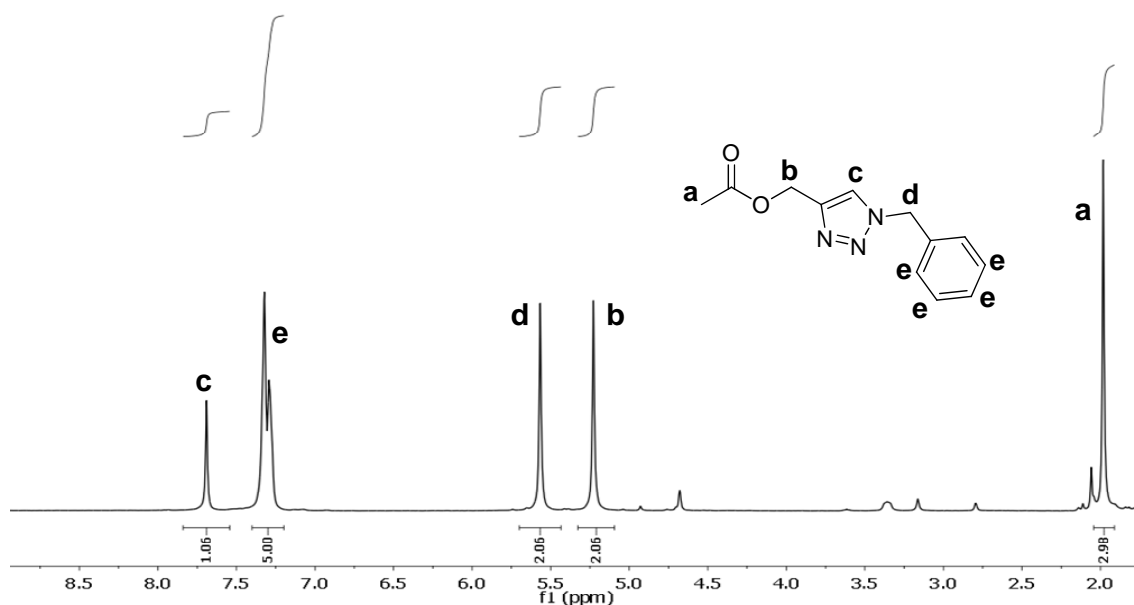


**Oxidative coupling of terminal alkynes:** To a mixture of  $\text{CuCl}_2$  (**1**) (3 mol% Cu) or **NP1** (5 mg, 0.5 mol% Cu) and  $\text{Et}_3\text{N}$  (3 mol%) the corresponding terminal alkyne (1.0 mmol) was added. The mixture was stirred at 60 °C for 8 h in air. After cooling to room temperature, the mixture was diluted with deuterated chloroform and filtered for characterization of the crude reaction medium through  $^1\text{H}$  NMR spectroscopy. The resulting 1,3-diyne product was isolated by removing the residual terminal alkyne through reduced pressure distillation and characterized by  $^1\text{H}$  NMR, GC and FTIR spectroscopy. The same procedures were followed during the dimerization of binary and ternary mixtures of alkynes.

**Synthesis of (1-benzyl-1*H*-1,2,3-triazol-4-yl) methyl acetate:** Propargyl acetate (1.0 mmol), benzyl azide (1.0 mmol) and  $\text{CuBr}$  (3 mol% Cu) were dissolved in chloroform (1.0 ml). The reaction mixture was degassed by passing argon for 15 min and then stirred at room temperature (r.t) for 2 h. Then, the mixture was diluted with chloroform and filtered for characterization of the crude reaction medium through  $^1\text{H}$  NMR spectroscopy.



The  $^1\text{H}$  NMR spectrum in  $\text{CDCl}_3$  of (1-benzyl-1*H*-1,2,3-triazol-4-yl) methyl acetate and the corresponding proton assignment is shown below:



## 2. Characterization Techniques

**$^1\text{H}$  Nuclear Magnetic Resonance ( $^1\text{H}$  NMR)** spectra were recorded at room temperature on Bruker spectrometers operating at 400 MHz or 500 MHz, using  $\text{CDCl}_3$  as solvent.

**Size-Exclusion Chromatography / Multi-Angle Laser Light Scattering (SEC/MALLS)** measurements were performed at 30 °C on an Agilent 1200 system equipped with PLgel 5 $\mu\text{m}$  Guard and PLgel 5 $\mu\text{m}$  MIXED-C columns, a differential refractive index (RI) detector (Optilab Rex, Wyatt) and a MALLS detector (MiniDawn Treos, Wyatt). Data analysis was performed with ASTRA Software from Wyatt. THF was used as eluent at a flow rate of 1 ml / min.  $\text{dn}/\text{dc}$  values in THF were determined using the Optilab Rex detector on line.

**Fourier Transform Infra-Red (FTIR) spectroscopy** spectra were recorded at room temperature on a JASCO 3600 FTIR spectrometer.

**Transmission Electron Microscopy (TEM)** measurements were performed using a high-resolution transmission electron microscope TECNAI G220 TWIN. The measurements were carried out using an accelerating voltage of 200 kV, under low dose conditions.

**Small Angle Neutron Scattering (SANS)** measurements were performed at the SANS-II instrument at the Swiss spallation neutron source SINQ, Paul Scherrer Institute, Villigen, Switzerland. Two incoming wavelengths ( $\lambda=10.5$  and  $5.27$  Å) and three different sample-detector distances (6, 4 and 1.2 m) were used. Solutions of the nanoparticles at 25 °C in DMF- $d_7$  at a concentration of 8 mg/ml were investigated in quartz cells of 2 mm thickness. The use of deuterated solvent greatly reduces the measuring time by significantly enhancing the scattering contrast. The results were corrected for background contributions applying the corresponding transmission factors.

**Thermal Gravimetric Analysis (TGA)** measurements were performed in a Q500-TA Instruments apparatus at a heating rate of 10 °C/min under nitrogen atmosphere from room temperature to 1000°C.

**X-ray photoelectron spectroscopy (XPS)** spectra were recorded at room temperature on a SPECS-XPS apparatus. Al  $K_{\alpha}$  X-ray line at 1486 eV was used. A **NP1** solution in chloroform (3 mg/ml) was added dropcast onto a Au/SiO<sub>2</sub> substrate, allowed to dry to form a thin film. The spectra were referenced to the SiO<sub>2</sub> signal of the substrate.

**Gas chromatography (GC)** was performed in a Shimadzu GC 14A gas chromatograph. The GC instrument was operated in split mode with a ratio of 40:5 and

the column head pressure was 100 kPa. The GC injector was maintained at 200°C and the detector at 200°C.

**Ultraviolet/visible (UV/Vis) spectroscopy** measurements were carried out at 25 °C in an Agilent 8453A apparatus with a Peltier thermostatic cell holder, T-controller 89090A.

### 3. Supporting Data

#### 3.1. Form factor of P1 and NP1 as determined by SANS measurements.

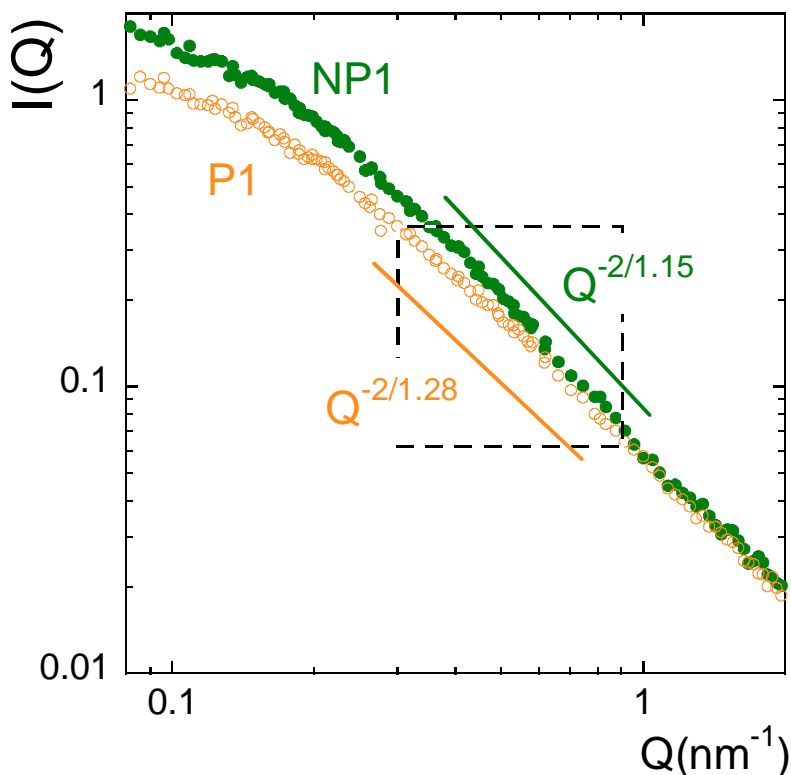


**Figure S1.** SANS results revealing the form factor of the metallo-folded SCNP **NP1** in solution when compared to precursor **P1**. Lines represent the asymptotic Ornstein–Zernike regime  $I(Q) \sim Q^{-2/\nu}$  ( $I$  = Intensity;  $Q$  = wavevector;  $\nu$  = scaling

exponent).<sup>[1]</sup> The exponent value for **NP1**,  $\nu = 1.15$ , is significantly higher than that expected for globular, compact nanoparticles,  $\nu = 0.66$  pointing to the non-compact conformation of **NP1** in solution. As an example, globular nano-objects such as native folded proteins do show a  $Q^{-2/0.66}$  scaling law. Due to the high molecular weight of the sample and the limited window of experimental  $Q$  values, reliable information about the actual radius of gyration and molar mass cannot be extracted with confidence from Figure S1.

### 3.2. Determination of the Cu content in NP1 from TGA data.

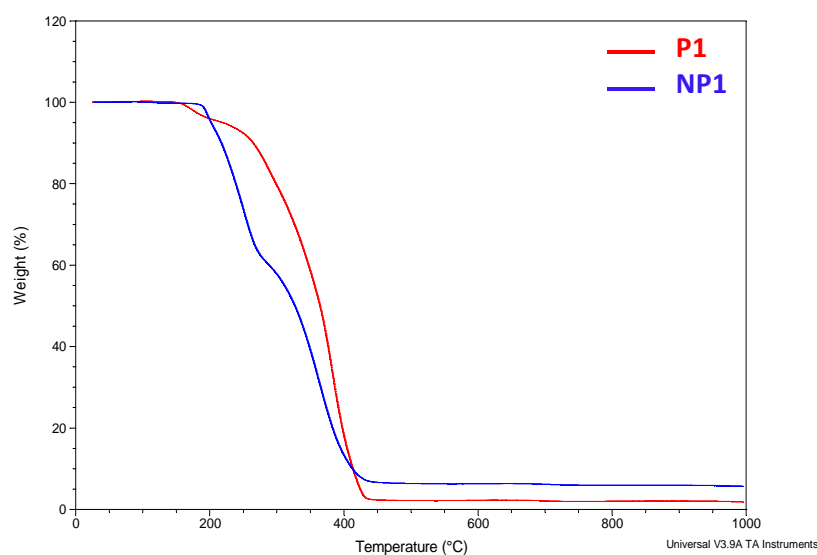


**Figure S2.** TGA curves for precursor **P1** (red line) and metallo-folded SCNP **NP1** (blue line). The content of copper in **NP1** was estimated from the residual weight that can be assigned to CuO species (6.6 wt%) due to the black color of the residues. It is worth noting that the precursor **P1**, which was taken as a control, was totally decomposed at temperatures above 450°C, so the residues observed for **NP1** can be only attributed to metal oxide species.

### 3.3. Determination of the oxidation state of Cu ions in NP1 from XPS measurements.

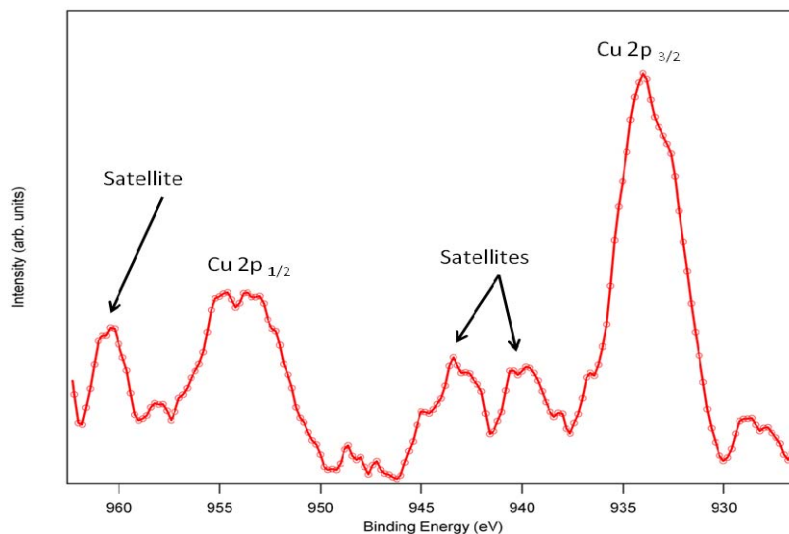


**Figure S3.** XPS spectrum showing the detailed Cu 2p region of **NP1**. The Cu 2p region exhibits a doublet structure with a separation of approximately 20 eV, due to the non-degenerate 2p ground state. The position of the  $2p_{3/2}$  and  $2p_{1/2}$  peaks could suggest either  $\text{Cu}^+$  or  $\text{Cu}^{2+}$  as there is a little difference in the binding energy position of these species<sup>[2]</sup>. However, the satellite peaks highlighted are characteristic of  $\text{Cu}^{2+}$ , indicating that the copper in **NP1** is in this oxidation state.<sup>[3, 4]</sup>

### 3.4. Illustrative alkyne dimerization experiments.

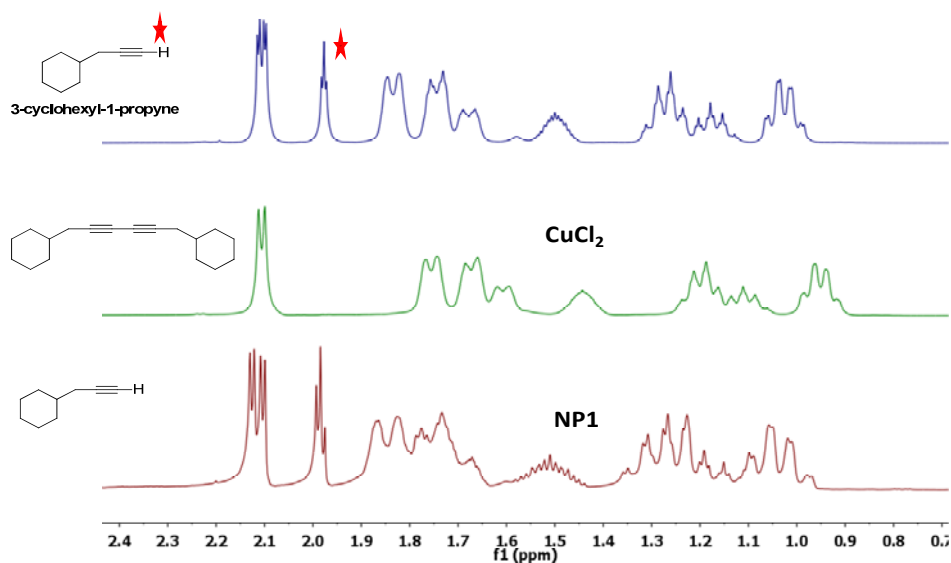


**Figure S4.**  $^1\text{H}$  NMR spectra of 3-cyclohexyl-1-propyne (**5a**) (blue line) in the region of the acetylenic proton (red asterisk) and the same spectral zone after reaction using  $\text{CuCl}_2$  (**1**) (blue curve) or metallo-folded SCNPs **NP1** (red curve) as catalysts. As can be seen in the spectra, with  $\text{CuCl}_2$  **5a** is consumed to the dimer (**5b**) whereas with **NP1** **5a** no reaction was observed.

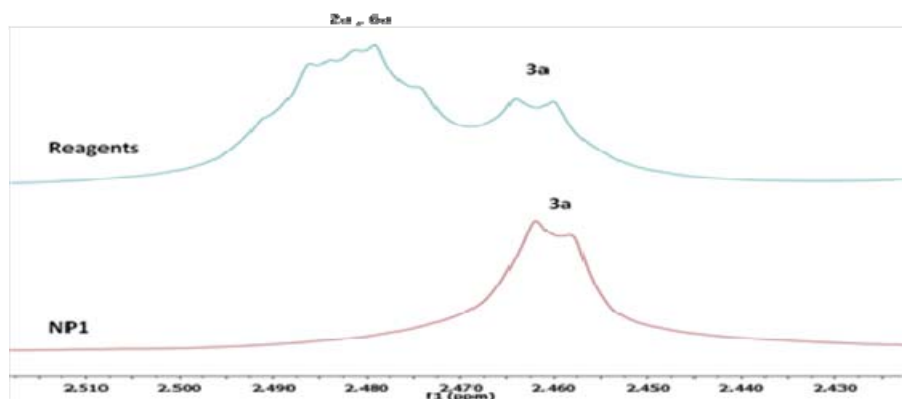


**Figure S5.**  $^1\text{H}$  NMR spectra showing signals from the acetylenic protons of the initial **2a** + **3a** + **6a** reagent mixture (blue curve) and the same spectral zone after reaction using metallo-folded SCNPs **NP1** as catalysts (red curve); the metallo-folded SCNP **NP1** remaining selective against **2a** and **6a**.

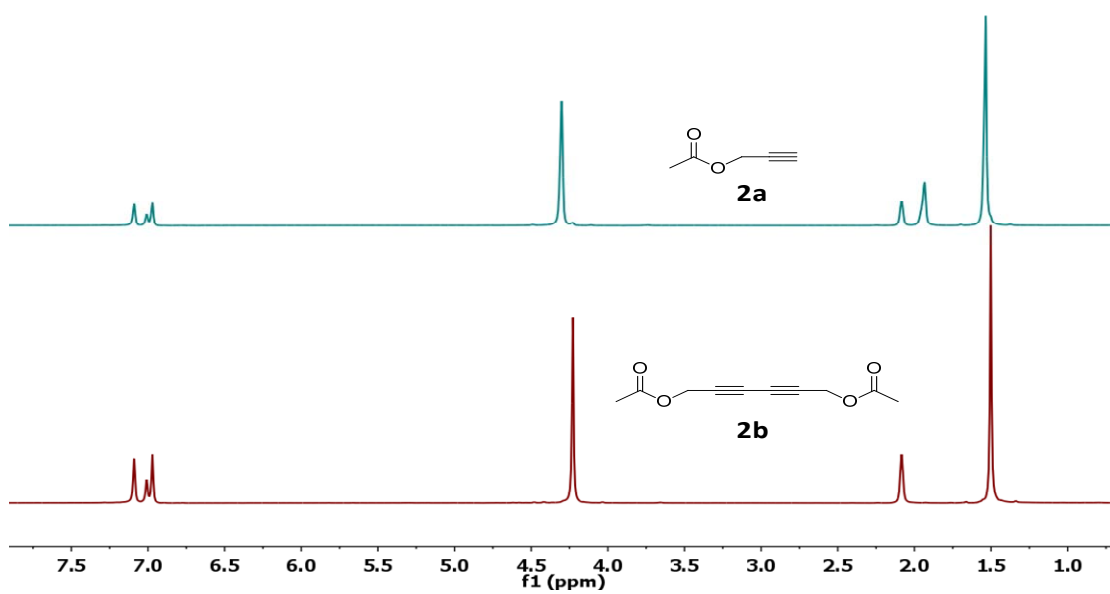


**Figure S6.** Synthesis of **2b** in solution:  $^1\text{H}$  NMR spectra corresponding to entry 11 in Table 1 of the main manuscript.

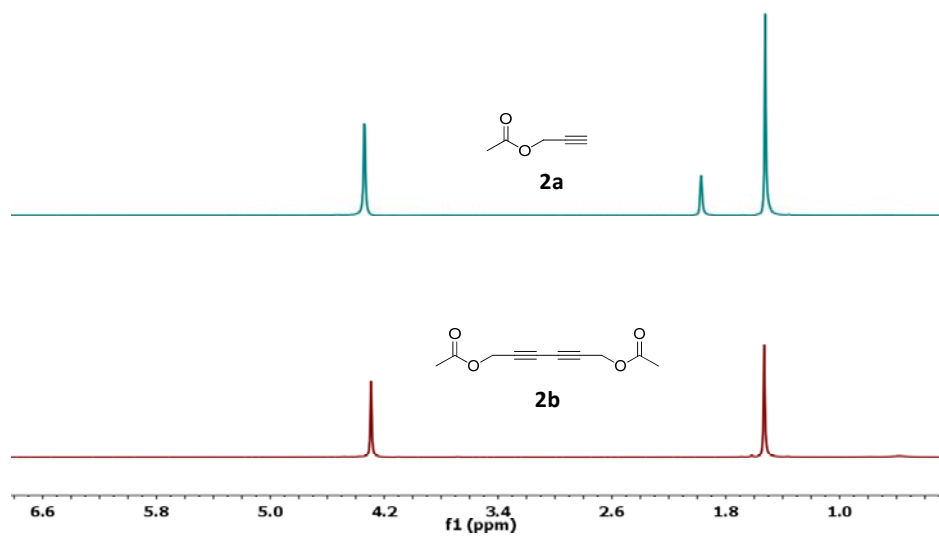


**Figure S7.**  $^1\text{H}$  NMR spectra recorded in benzene- $\text{d}_6$  solvent corresponding to initial reagent **2a** and product **2b** after reaction in bulk conditions.

### 3.5 Propargyl acetate oxidative coupling catalyzed by NP1: Kinetics data.

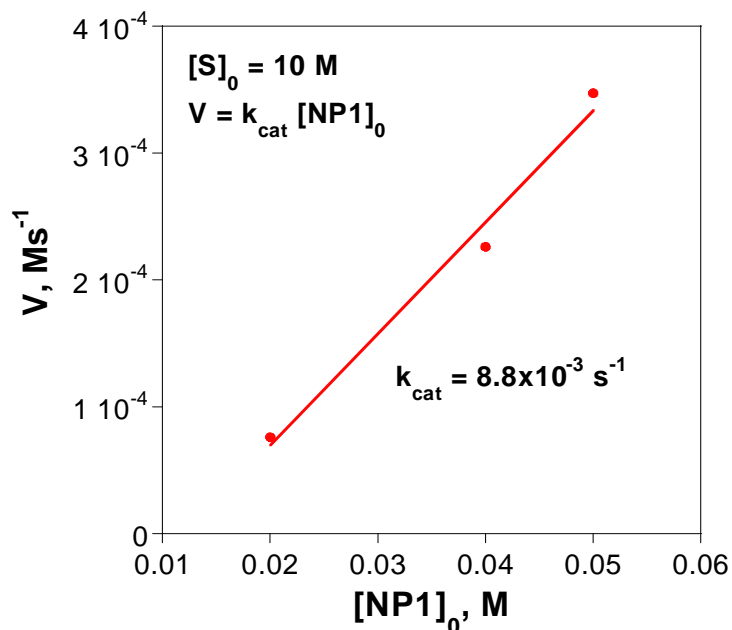


**Figure S8.** Analysis of kinetics data to determine the apparent catalytic constant ( $k_{cat}$ ) for propargyl acetate dimerization catalyzed by **NP1**. The initial concentration of propargyl acetate was  $[S]_0 = 10 \text{ M} \gg [NP1]_0$  ( $[NP1]_0$  from 0.02 M to 0.05 M). Under such conditions the classical Michaelis-Menten equation becomes  $V = d[P]/dt = k_{cat} [NP1]_0$  ( $[S]_0 / (K_M + [S]_0) \approx k_{cat} [NP1]_0$  by assuming  $K_M \ll [S]_0$  where  $V = d[P]/dt$  is the rate of reaction determined, as usual, from the initial slope of a plot of  $[P]$  versus time, at constant concentration of **NP1**, and  $K_M$  is the substrate concentration at which the reaction rate is half of the maximum reaction rate.

### 3.6 Additional alkyne dimerization experiments.

**Table S1.** Additional control reactions.

Entry	Catalyst <sup>a</sup>	Reagents	Products <sup>b</sup>	Yield (%) <sup>b</sup>	Selectivity
1	NP1	10a	10b	0	-
2	NP1	11a	11b	0	-
3	NP1	2a <sup>c</sup>	2b	33 <sup>c</sup>	-
4	Cu(acac) <sub>2</sub> <sup>d</sup>	2a	2b	0	-
5	NP1	2a+3a+4a <sup>e</sup>	2b <sup>f</sup>	>98 <sup>g</sup>	Yes

<sup>a</sup> Reaction conditions: solvent-free unless stated, 1 mmol of alkyne, Et<sub>3</sub>N (3 mol%), NP1: 0.5 mol% Cu, 60 °C, 8 h, air. <sup>b</sup> From GC and <sup>1</sup>H NMR data. <sup>c</sup> Diluted with ethyl acetate to half of the original alkyne concentration. <sup>d</sup> The concentration of Cu(acac)<sub>2</sub> was increased to 3 mol%. <sup>e</sup> Diluted with benzene to half of the original total alkyne concentration. <sup>f</sup> No by-products from cross-coupling reactions were detected. <sup>g</sup> Referred to **2a**.

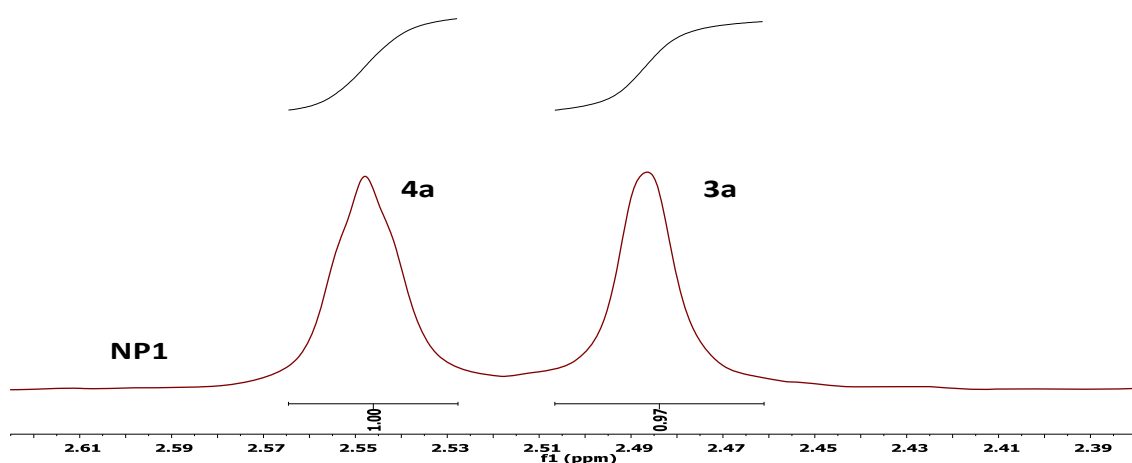


**Figure S9.** Selectivity of **2a+3a+4a** in solution: <sup>1</sup>H NMR spectrum in benzene-d<sub>6</sub> corresponding to entry 5 in Table 1. The metallo-folded SCNP NP1 remains selective towards **2a**.

### 3.7 Investigation about potential Cu(I) formation after alkyne dimerization

In order to investigate the potential formation of Cu(I) species after alkyne dimerization, the electronic absorption spectra of **NP1** was recorded at the beginning and at the end of the reaction.

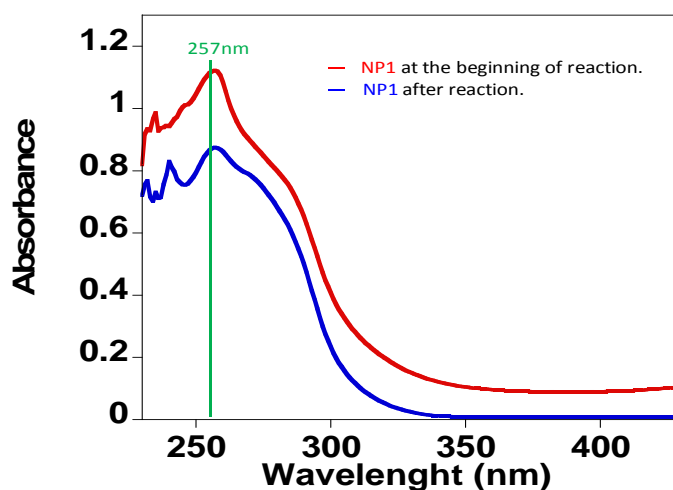


**Figure S10.** UV-Vis spectra of **NP1** in chloroform at the beginning and at the end of the reaction. Even if both spectra show a maximum at about 257 nm, some changes in the shape of the spectrum are observed that potentially could be attributed to the generation of Cu(I) species.

To further investigate this issue, the synthesis of (1-benzyl-1*H*-1,2,3-triazol-4-yl) methyl acetate was attempted with SCNPs **NP1** that were used before in the synthesis of **2b**. As illustrated in Figure S11, the formation of (1-benzyl-1*H*-1,2,3-triazol-4-yl) methyl acetate in very low yield (6 %) suggests the potential presence of only a minor amount of Cu(I) in SCNPs **NP1** after alkyne dimerization.

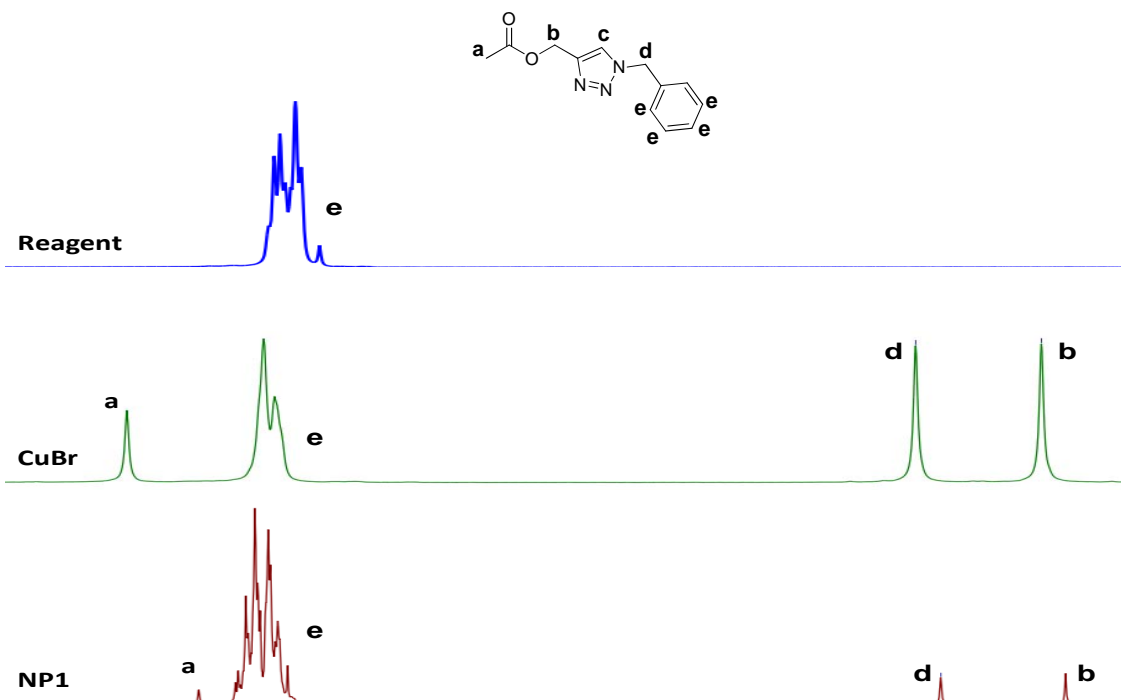


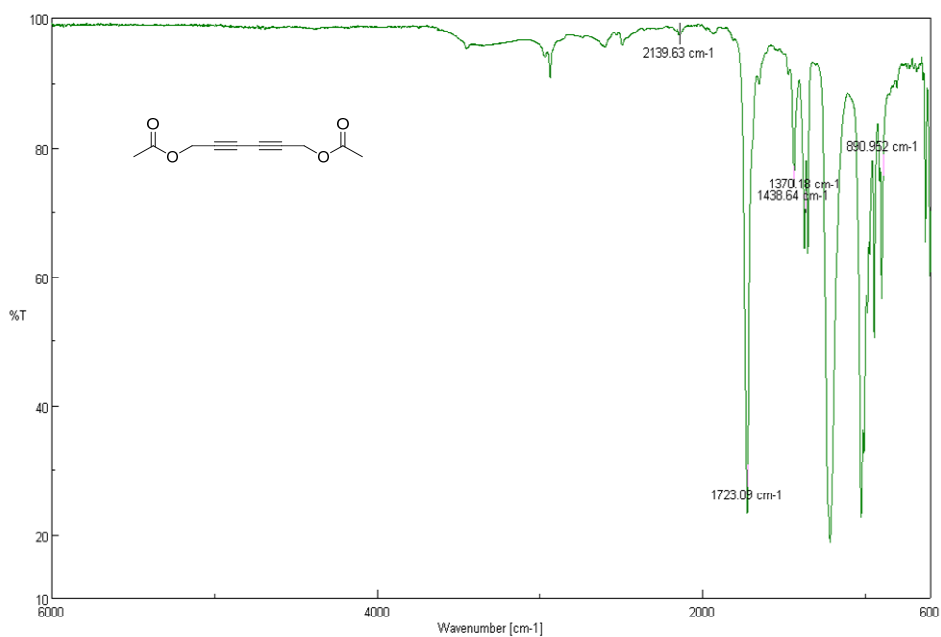
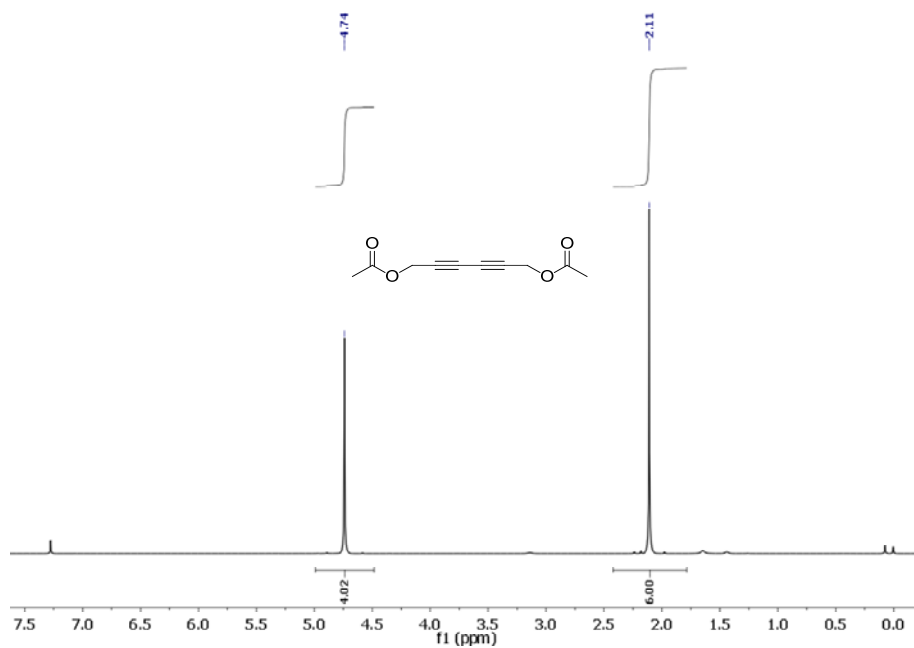
**Figure S11.** Blue trace is the <sup>1</sup>H NMR spectrum of benzyl azide in the region of the aromatic protons at the beginning of the reaction. Green trace is the <sup>1</sup>H NMR spectrum corresponding to the formation of (1-benzyl-1*H*-1,2,3-triazol-4-yl) methyl acetate using CuBr as “click” chemistry catalyst. Red trace is the <sup>1</sup>H NMR spectrum corresponding to the formation of (1-benzyl-1*H*-1,2,3-triazol-4-yl) methyl acetate (yield 6 %) using SCNP **NP1** that was used before in the synthesis of **2b**.

### 3.8 Spectral data of the 1,3-diynes synthesized in this work.

#### Hexa-2,4-diyne-1,6-diyl diacetate (**2b**)<sup>[5]</sup>

<sup>1</sup>H NMR (400 MHz, CDCl<sub>3</sub>): δ (ppm) = 4.74 (s, 4H), 2.11 (s, 6H).

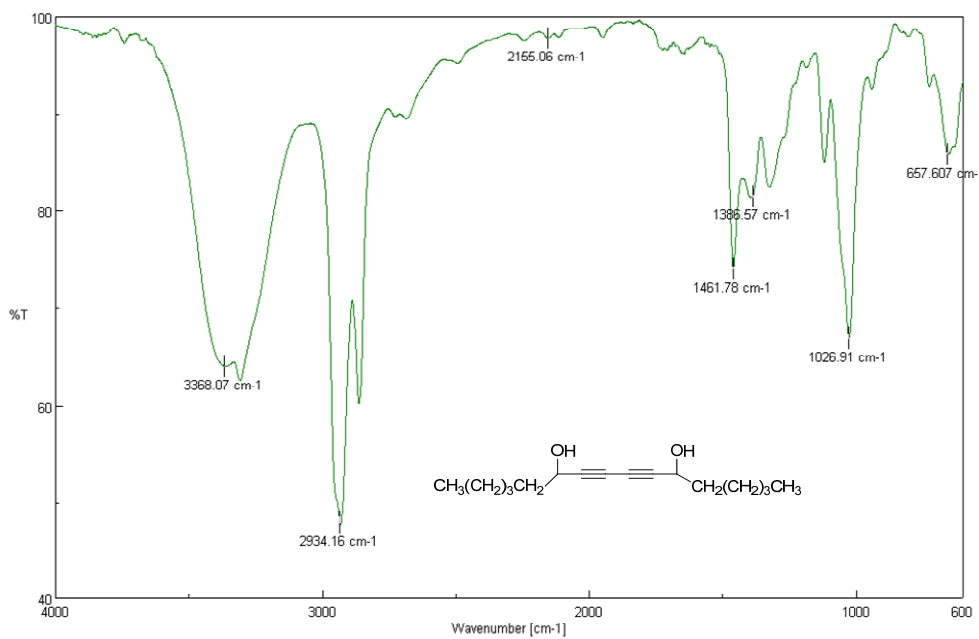
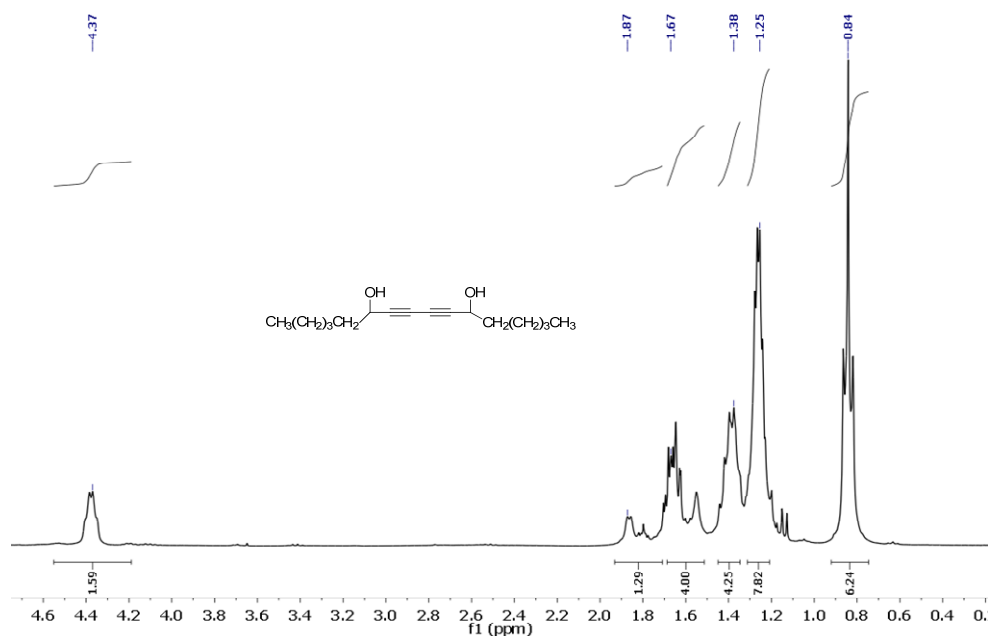
IR (KBr): 2139, 1723, 1438, 1370, 890 cm<sup>-1</sup>.



### Hexadeca-7,9-diyne-6,11-diol (3b)<sup>[6]</sup>

<sup>1</sup>H NMR (400 MHz, CDCl<sub>3</sub>) : δ (ppm) = 4.37 (m, 2H), 1.87 (s, 2H of hydroxyl), 1.67 (m, 4H), 1.38 (m, 4H), 1.25 (m, 8H), 0.84 (t, 6H).

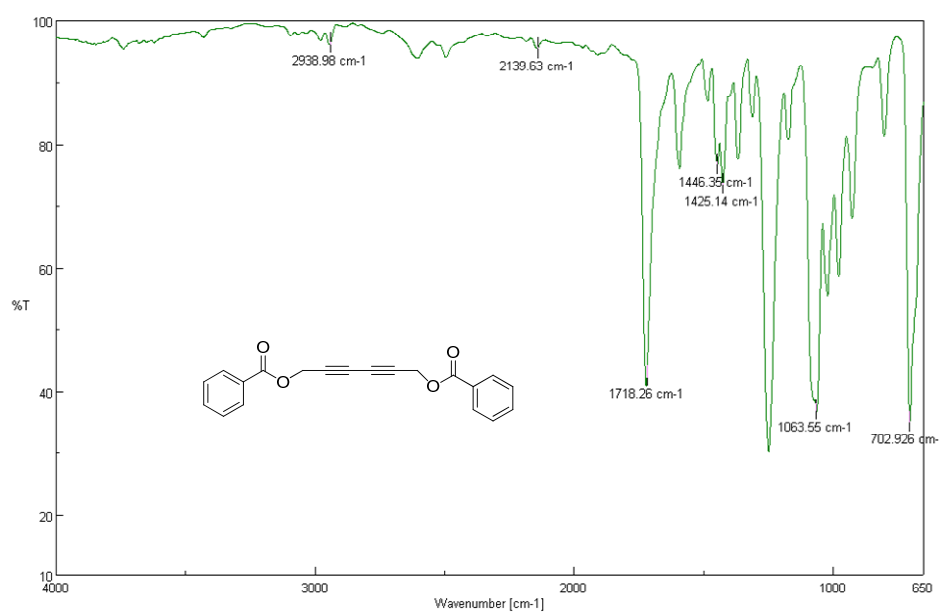
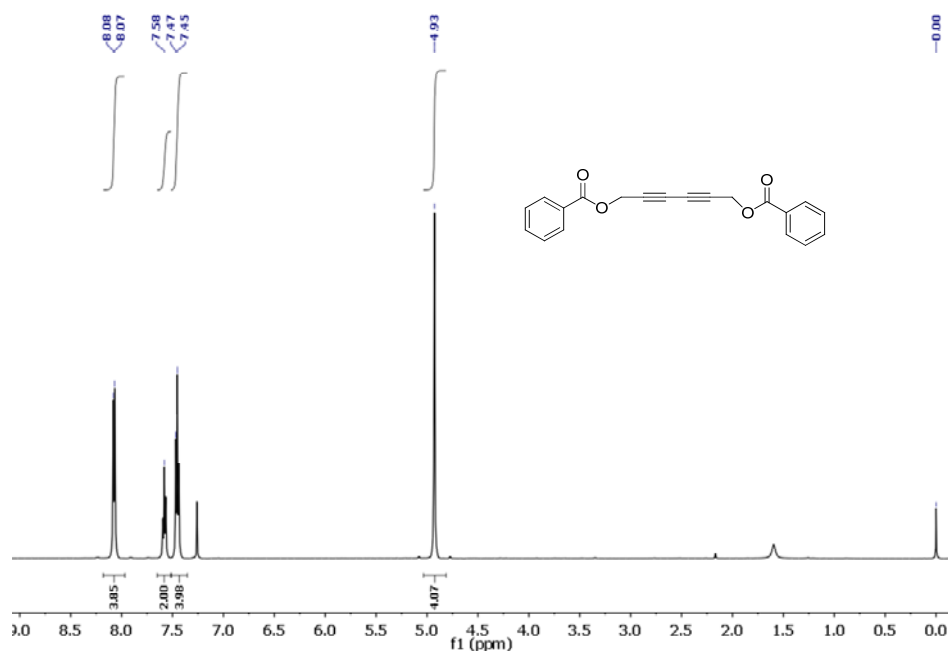
IR (KBr): 3368 (O-H Str), 2934, 2155, 1461, 1386, 1026, 657 cm<sup>-1</sup>.



**2,6-Hexadiyne-1,6-diol,1,6-dibenzoate (4b)**<sup>[7]</sup>

<sup>1</sup>H NMR (400 MHz, CDCl<sub>3</sub>) :  $\delta$  (ppm) = 8.08 (m, 4H), 7.58 (m, 2H), 7.45 (m, 4H), 4.93 (s, 4H).

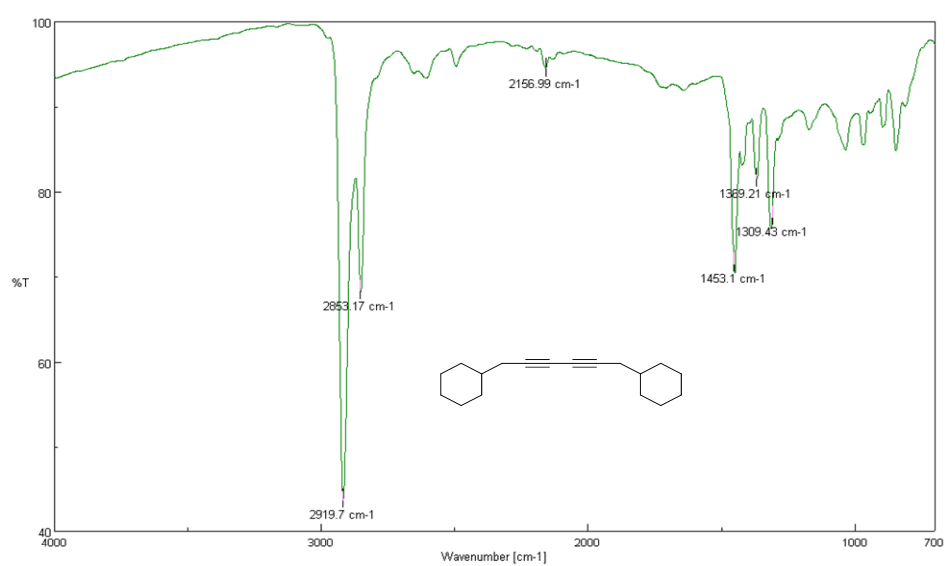
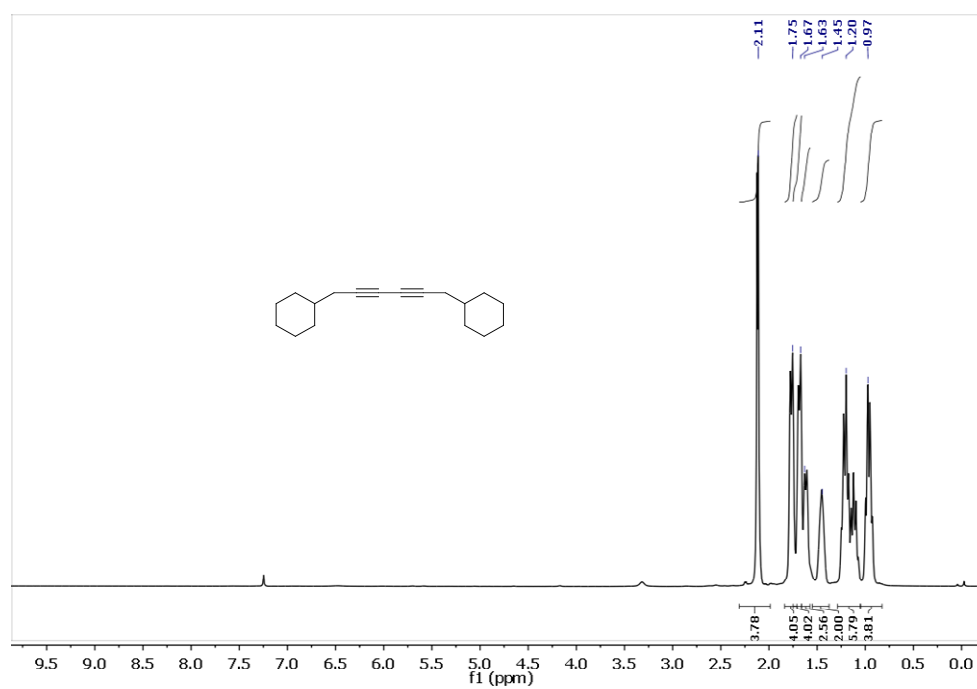
IR (KBr): 2938, 2139, 1718, 1446, 1425, 1063, 702 cm<sup>-1</sup>.



**1,6-dicyclohexylhexa-2,4-diyne (5b)**<sup>[8]</sup>

<sup>1</sup>H NMR (400 MHz, CDCl<sub>3</sub>) :  $\delta$  (ppm) = 2.11 (m, 4H), 1.75 (m, 4H), 1.67 (m, 4H), 1.63 (m, 2H), 1.45 (m, 2H), 1.20 (m, 6H), 0.97 (m, 4H).

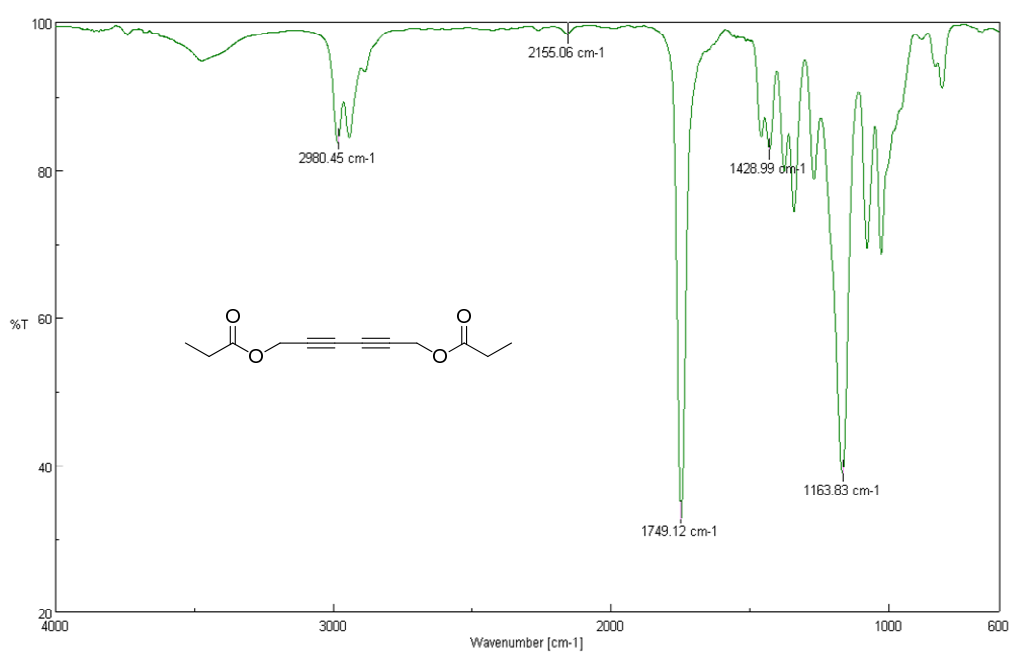
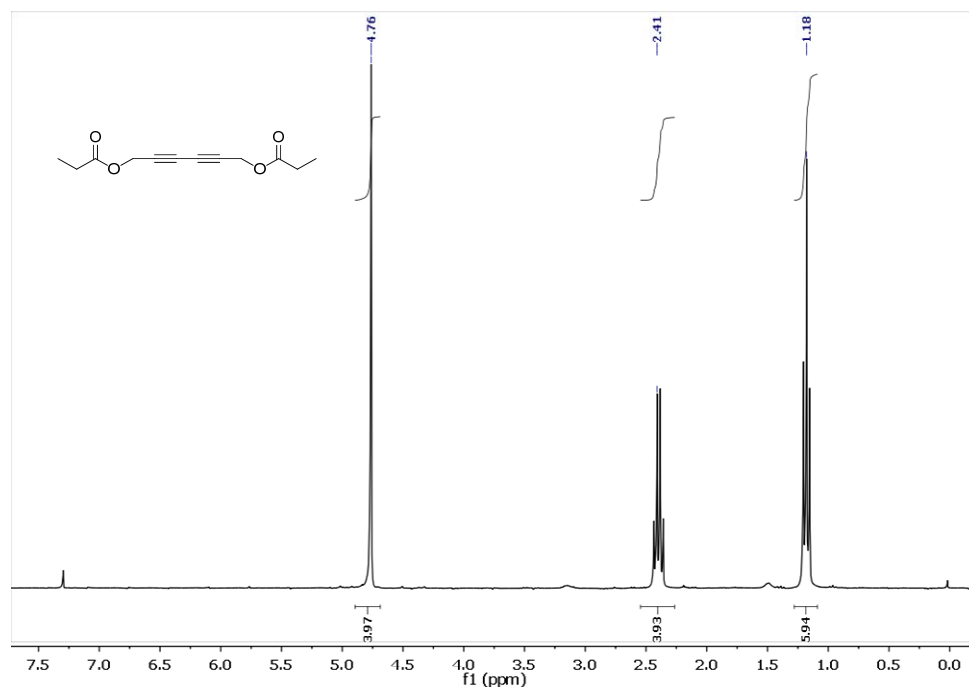
IR (KBr): 2919, 2853, 2156, 1453, 1369, 1309 cm<sup>-1</sup>.



**Hexa-2,4-diyne-1,6-diyl dipropionate (6b)<sup>[9]</sup>**

<sup>1</sup>H NMR (400 MHz, CDCl<sub>3</sub>) : δ (ppm) = 4.76 (s, 4H), 2.41 (m, 4H), 1.18 (m, 6H).

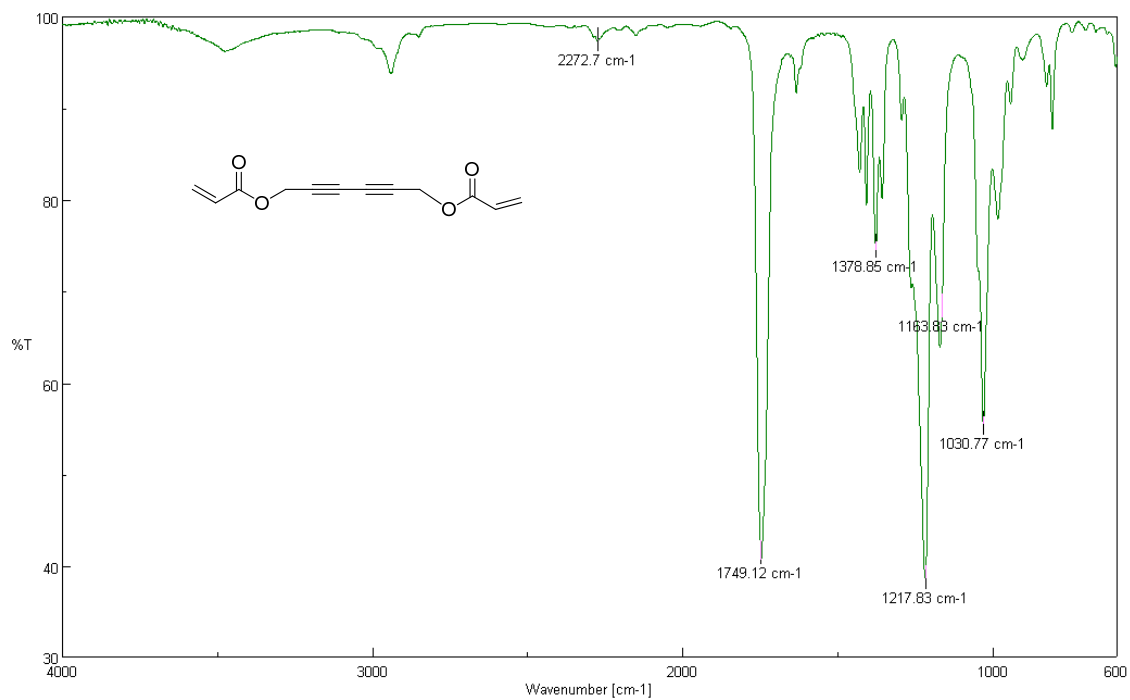
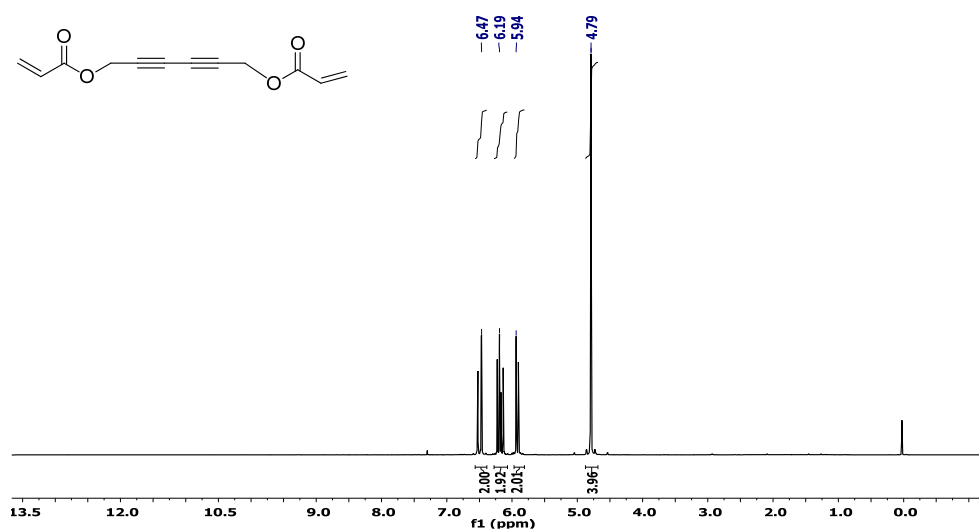
IR (KBr): 2980, 2155, 1749, 1428, 1163 cm<sup>-1</sup>.



## Hexa-2,4-diyne-1,6-diyl diacrylate (7b)

$^1\text{H NMR}$  (400 MHz,  $\text{CDCl}_3$ ):  $\delta$  (ppm) = 6.47 (d, 2H), 6.19 (m, 2H), 5.94 (d, 2H), 4.79 (s, 4H).

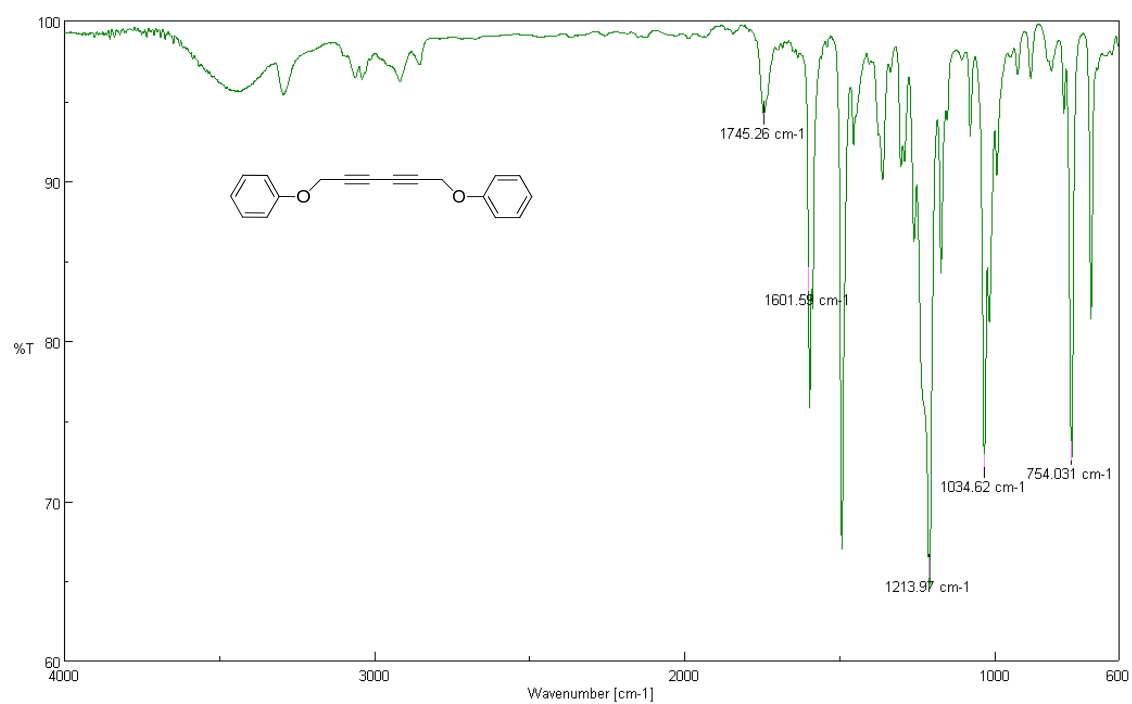
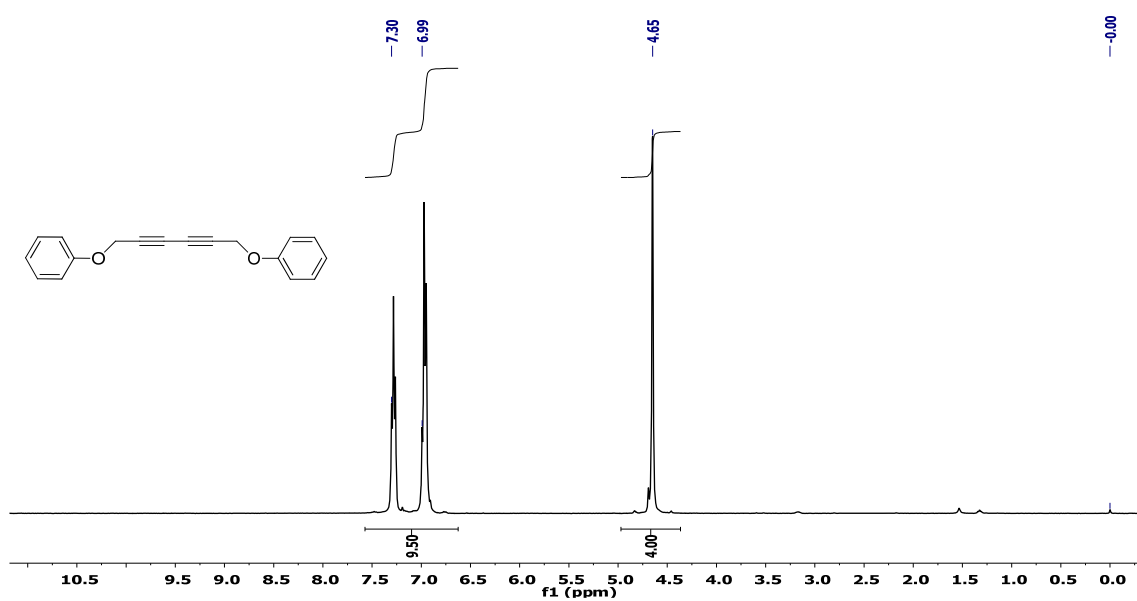
IR (KBr): 2272, 1749, 1378, 1217, 1163, 1030  $\text{cm}^{-1}$ .



**1,6-Diphenoxyhexa-2,4-diyne (9b)**<sup>[10]</sup>

<sup>1</sup>H NMR (400 MHz, CDCl<sub>3</sub>) : δ (ppm) = 7.3 and 6.99 (m, 10H), 4.65 (s, 4H).

IR (KBr): 1745, 1601, 1213, 1034, 754 cm<sup>-1</sup>.



#### 4. References

- [1] Rubinstein, M.; Colby, R. H. *Polymer Physics*; Oxford University Press: New York, **2003**.
- [2] Xiao W. *et al. J. Phys.: Condens. Matter.* **2003**, *15*, 1155.
- [3] Kumar R. S. *et al. Micropor. Mesopor. Mat.* **2013**, *168*, 57.
- [4] Cioffi N. *et al. Chem. Mater.* **2005**, *17*, 5255.
- [5] Zhang S. *et al. Adv. Synth. Catal.* **2011**, *353*, 1463.
- [6] Setzer W. N. *et al. Chem. Pharm. Bull.* **2000**, *48*, 1776.
- [7] Xu R. *et al. J. Am. Chem. Soc.* **2006**, *128*, 5541.
- [8] Chen Z. *et al. J. Org. Chem.* **2010**, *75*, 6700.
- [9] Makhsumov A. G. *et al. Uzbekskii Khimicheskii Zhurnal* **1985**, *1*, 36.
- [10] Feng X. *et al. J. Organomet. Chem.* **2011**, *696*, 1479.